Vol 17 No 7, July 2008
1674-1056/2008/17(07)/2484-07

Chinese Physics B

© 2008 Chin. Phys. Soc.
and IOP Publishing Ltd

Theoretical research on the performance of a practical helix travelling wave tube*

Duan Zhao-Yun(段兆云)†, Gong Yu-Bin(宫玉彬),
Wei Yan-Yu(魏彦玉), and Wang Wen-Xiang(王文祥)

Vacuum Electronics National Laboratory, College of Physical Electronics, University of Electronic Science and Technology of China, Chengdu 610054, *China*

(Received 26 March 2007; revised manuscript received 6 March 2008)

On the basis of a rigorous field theory, two different physical models of attenuator and sever have been proposed. One is named High attenuation (HATT) model in which both attenuator and sever are considered as a unified attenuator, but the sever is regarded as an area of very high loss; the other is called Sever and attenuator (SATT) model in which the sever is modelled as a drift area in which the electric and magnetic fields both vanish. A complex function is derived and potential sinking effect is also considered. Thus, a set of more practical self-consistent equations of nonlinear beam–wave interaction is formulated. Simulations are carried out under the conditions of the two different physical models, and the simulation results are compared with the experimental data. The results show that in the case of single signal drive, the unknown second harmonic should be included for predicting the saturated output power. It is also evident that the SATT model and the HATT model predict the same physical nature, whereas the results predicted by the HATT model are much closer to the experimental data than those obtained from the SATT model. Therefore, these results provide a strong theoretical basis for designing broadband and high gain helix travelling wave tubes.

Keywords: helix, travelling wave tube, field theory, nonlinear beam–wave interaction
PACC: 4100, 4180D

1. Introduction

High power microwave devices are widely applied to radar, communications and electronic warfare.[1−3] As a high power microwave device, the travelling wave tube (TWT) is broadly studied. As is known, both linear and nonlinear theories used to analyse the beam–wave interaction in a TWT have been developed since the pioneering work of Pierce and co-workers.[4] In fact, the beam–wave interaction in a TWT is essentially nonlinear, so the nonlinear theory of a TWT has developed early in the literature,[5−9] and in general, it can be grouped into two main classes. One is transmission line equivalent circuit method;[8] the other is guided wave excited theory.[9] All these methods have been widely used to design a TWT, but in order to further eliminate many trial and erroneous fabrications as well as test steps, new interest is renewed to study the beam–wave interaction. GATOR code,[10] CHRISTINE code,[11,12] MUSE code,[13] and other methods have appeared. In China, the relevant research work on the TWT has also been conducted.[14−18]

In this paper, we study the beam–wave interaction in a helix TWT based on the novel beam–wave interaction theory,[11] in which the attenuator and the sever were not clearly considered. However, there exist the attenuator and the sever in a practical helix TWT for improving the output power/gain and suppressing the parasitic oscillations.[19] In order to further improve this theory, first, two different physical models of attenuator and sever are set up one is: the model, named High attenuation (HATT) model, in which both attenuator and sever are considered as a unified attenuator; the other is the model, called Sever and attenuator (SATT) model, in which the sever is modelled as a drift area in which the electric and magnetic fields are simultaneously considered to be zero. Next, the concrete expression of the complex function is derived. As a result, a set of more practical self-consistent equations of the nonlinear beam–wave interaction is set up. Finally, we carry out numerical calculations, and we find that the results are in good agreement with the experimental results.

*Projects partially supported by the National Natural Science Foundation of China (Grant Nos 60601007 and 60532010), and the Youth Science and Technology Foundation of University of Electronic Science and Technology of China (Grant No JX05018).
†E-mail: zhyduan@uestc.edu.cn

2. The general formulation

2.1. RF characteristics of helical slow wave structure (SWS)

Prior to predicting helix TWT performances, RF characteristics of helical SWS should be accurately computed. Tape model taking into account the space harmonics generated due to the axial periodicity of the structure, which would yield more accurate results than the sheath–helix model, is adopted in this paper. Also, surface currents on the tape helix, of which the initial guess has been eliminated, are expanded into a series of Chebyshev polynomials. Besides the models for treating the finite radial thickness of helix, such as the Swift–Hook model,[19] in which a free-space gap equal to half the helix thickness is considered between the mean helix radius and the outer helix radius, and the Yan model,[18] in which a free-space gap is considered between the inner and the outer helix radii within which the fields are constant, which effectively implies the presence of two sheath helices: one is at the inner helix radius and the other is at the outer helix radius, or combination of these two models, the Swift–Hook model is found to be the simplest and valid for a wide range of SWS parameters. This motivates the authors, in the present analysis, to choose the Swift–Hook model for the finite thickness of the helix which is further modelled by the tape–helix model. As a result, based on a rigorous field theory, the dispersion relation and the interaction impedance can be expressed as follows, respectively:[17]

$$\begin{pmatrix} \tilde{M}_{00} & \tilde{M}_{01} & \tilde{M}_{02} & \cdots \\ \tilde{M}_{10} & \tilde{M}_{11} & \tilde{M}_{12} & \cdots \\ \tilde{M}_{20} & \tilde{M}_{21} & \tilde{M}_{22} & \cdots \\ \cdots & \cdots & \cdots & \cdots \end{pmatrix} \begin{pmatrix} J_{\xi 0} \\ J_{\eta 0} \\ J_{\xi 1} \\ J_{\eta 1} \\ \cdots \end{pmatrix} = \tilde{M}\tilde{J} = 0, \tag{1}$$

where matrix $\tilde{M}_{ll'}(l, l' = 0, 1, 2, \cdots \infty)$ can be defined as

$$\tilde{M}_{ll'} = (-1)^l j^{l+l'} \sum_{n=-\infty}^{\infty} \begin{pmatrix} J_l(\alpha_n) & 0 \\ 0 & \frac{l+1}{\alpha_n} J_{l+1}(\alpha_n) \end{pmatrix} \begin{pmatrix} \cos\psi & \sin\psi \\ -\sin\psi & \cos\psi \end{pmatrix} \tilde{Z}_n \begin{pmatrix} 0 & 1 \\ -1 & 0 \end{pmatrix} T_{ll'},$$

and

$$T_{ll'} = \begin{pmatrix} \cos\psi & -\sin\psi \\ \sin\psi & \cos\psi \end{pmatrix} \begin{pmatrix} J_l(\alpha_n) & 0 \\ 0 & \frac{l'+1}{\alpha_n} J_l(\alpha_n) \end{pmatrix}, \tag{2}$$

with $\alpha_n = W/2\,(n/(a\sin\psi) + \beta\cos\psi)$,$J_l(\alpha_n)$ being the Bessel function of the first kind, and

$$K(r) = \frac{\left|E_{zn}^{(1)}(r)\right|^2}{2\beta_n^2 P}, \tag{3}$$

where P denotes the power flowing along the tape helix and can be written as

$$\begin{aligned} P =& \mathrm{Re}\left(\frac{1}{2}\int \boldsymbol{E}\times\boldsymbol{H}^*\mathrm{d}s\right) = \mathrm{Re}\left(\pi\sum_{n=-\infty}^{\infty}\int_0^b r\mathrm{d}r(E_{rn}H_{\theta n}^* - E_{\theta n}H_{rn}^*)\right) \\ =& \mathrm{Re}\left(\sum_{i=1}^{N+2}\sum_{n=-\infty}^{\infty}(P_n^{(i)}(a^{(i)}) - P_n^{(i)}(a^{(i-1)}))\right) \end{aligned} \tag{4}$$

with

$$\begin{aligned} P_n^{(i)}(r) &= \frac{\pi\omega\varepsilon_0\beta_n}{\gamma_n^{(i)4}}(\varepsilon_r^{(i)}P_1 + \eta_0^2 P_2 + jn\eta_0 P_3), \\ P_1 &= \left(rE_{zn}^{(i)*}\tfrac{\partial}{\partial r}E_{zn}^{(i)} - \tfrac{1}{2}(\gamma_n^{(i)2}r^2 + n^2)|E_{zn}^{(i)}|^2 + \tfrac{1}{2}r^2|\tfrac{\partial}{\partial r}E_{zn}^{(i)}|^2\right), \\ P_2 &= rH_{zn}^{(i)*}\frac{\partial}{\partial r}H_{zn}^{(i)} - \frac{1}{2}(\gamma_n^{(i)2}r^2 + n^2)|H_{zn}^{(i)}|^2 + \frac{1}{2}r^2\left|\frac{\partial}{\partial r}H_{zn}^{(i)}\right|, \\ P_3 &= \varepsilon_r^{(i)}\frac{\omega}{\beta_n c}E_{zn}^{(i)*}H_{zn}^{(i)} - \frac{\beta_n c}{\omega}E_{zn}^{(i)}H_{zn}^{(i)*}. \end{aligned} \tag{5}$$

2.2. The derivation of the complex function

In the literature,[11] both the field equation and the motion equation include the complex function $e_2(z)$. However, the concrete expression of the complex function is unknown. Hence, its concrete expression is derived by using the following method in order to effectively use the nonlinear beam–wave interaction theory.

If we consider the fields within an imaginary cylinder centred on the z-axis, with a radius less than that of the helix, then the functional forms of $\boldsymbol{e}(x)$ and $\boldsymbol{b}(x)$, which are dimensionless solutions to Maxwell equations for frequency ω and wave number of the fundamental wave in the axial direction $k_z(z)$, can be simply expressed in cylindrical coordinates. In particular, if the fields are assumed to be helically symmetrical and the Floquet theorem is also applied, then for a certain input signal, the z-components of the normalized electric and magnetic fields are written as

$$e_z(r,\theta,z) = \sum_{m=-\infty}^{\infty} e_{zm}(r)\exp[-\mathrm{i}m(\theta - k_{\mathrm{H}}z)], \tag{6a}$$

$$b_z(r,\theta,z) = \sum_{m=-\infty}^{\infty} b_{zm}(r)\exp[-\mathrm{i}m(\theta - k_{\mathrm{H}}z)], \tag{6b}$$

where $k_{\mathrm{H}} = 2\pi/\lambda_{\mathrm{h}}$, λ_{h} is the helix pitch, m is the number of the space harmonic wave, and e_{zm} and b_{zm} are complex amplitudes, respectively.

According to the longitudinal field method,[21] the transverse field components are expressed as

$$e_{rm}(r) = \frac{1}{\gamma_m^2}\left[-\mathrm{i}k_{zm}\frac{\partial e_{zm}(r)}{\partial r} - \frac{m}{r}\frac{\omega}{c}b_{zm}(r)\right], \tag{7a}$$

$$e_{\theta m} = \frac{1}{\gamma_m^2}\left[-\frac{m}{r}k_{zm}e_{zm}(r) + \mathrm{i}\frac{\omega}{c}\frac{\partial b_{zm}(r)}{\partial r}\right], \tag{7b}$$

$$b_{rm} = \frac{1}{\gamma_m^2}\left[\frac{m}{r}\frac{\omega}{c}e_{zm}(r) - \mathrm{i}k_{zm}\frac{\partial b_{zm}(r)}{\partial r}\right], \tag{7c}$$

$$b_{\theta m} = \frac{1}{\gamma_m^2}\left[-\mathrm{i}\frac{\omega}{c}\frac{\partial e_{zm}(r)}{\partial r} - \frac{m}{r}k_{zm}b_{zm}(r)\right], \tag{7d}$$

where $k_{zm} = k_z + mk_{\mathrm{H}}$ and $\gamma_m^2 = k_{zm}^2 - \dfrac{\omega^2}{c^2}$ is the square of the radial propagation factor with c being the speed of light in vacuum.

The axial components of the electric and the magnetic fields have simple representations in any region containing the origin. These are

$$e_{zm}(r) = e_{zm}^{(0)}I_m(\gamma_m r), \tag{8a}$$

and

$$b_{zm}(r) = b_{zm}^{(0)}I_m(\gamma_m r), \tag{8b}$$

where $e_{zm}^{(0)}$ and $b_{zm}^{(0)}$ are constants, and $I_m(\gamma_m r)$ is the first modified Bessel function of order m and argument $\gamma_m r$.

In a one-dimensional model, only $e_{zm}^{(0)}$ is needed and it may be expressed in terms of the interaction impedance for mth spatial harmonic at radius r, i.e.

$$K_m(r) \equiv \frac{\left|2\dfrac{\omega}{c}\delta A_m e_{zm}(r)\right|^2}{2k_m^2 P_m} = \frac{4\pi}{c}\frac{|e_{zm}(r)|^2}{k_m^2 A_{\mathrm{eff},m}}. \tag{9}$$

Expression (8a) is inserted into expression (9), yielding

$$A_{\mathrm{eff},m}|e_{zm}^{(0)}| = \frac{k_m}{I_m(\gamma_m r)}\left(\frac{K_m(r)}{4\pi/c}\right)^{1/2}, \tag{10}$$

where $A_{\mathrm{eff},m}$ is the effective cross-section area.

According to expression (10) and the definition of the complex function $e_2(n,z)$, after mathematical manipulations and the rearranging of terms, $e_2(z)$ is obtained as

$$e_2(z) = \frac{k_z}{r_{\mathrm{bo}} - r_{\mathrm{bi}}}\int_{r_{\mathrm{bi}}}^{r_{\mathrm{bo}}}\left[\frac{K(r)}{4\pi/c}\right]^{1/2}\mathrm{d}r \times \exp\left[\mathrm{i}\int_0^z (k_z(z') - \omega/v_{z0})\mathrm{d}z'\right], \tag{11}$$

where r_{bi} and r_{bo} are the inner radius and the outer radius in the beam discs, respectively, and v_{z0} is the initial axial speed of a particle.

2.3. Two different physical models

Attenuator and sever always exist in a practical helix TWT and may be described by using two different models: HATT model and SATT model. In the above two models, the phase speed and the interaction impedance are considered as constants and identical with those in the input section adjacent to the attenuator. For the first model, i.e. HATT model, the attenuation constant results from the attenuator and sever, while the second model, i.e. SATT model, the attenuation constant originates only from the attenuator. Thus, for the first model, the self-consistent equations of the nonlinear beam–wave interaction considering the attenuator and sever can be modified into field equation

$$\left(\frac{\mathrm{d}}{\mathrm{d}z} + \alpha_t(z)\right)a(z) = \frac{2\pi\mathrm{i}I}{I_A}e_2^*(z)\langle \mathrm{e}^{-\mathrm{i}\psi}\rangle, \tag{12}$$

where the total attenuation coefficients $\alpha_t(z) = \alpha_0(z) + \alpha_a(z)$ with $\alpha_0(z)$ being the loss of the circuits and $\alpha_a(z)$ the attenuation of the attenuator or

sever; $a(z)$ is the normalized field amplitude; I is the beam current; $I_{\rm A}$ is equal to 1.7×10^4A; ψ_n is the phase relative to the nth signal.

Phase evolving equation is expressed as

$$\frac{{\rm d}\psi}{{\rm d}z}=\omega(1/v_{z0}-1/v_z), \tag{13}$$

where v_z denote the axial speeds of a particle at time t.

Motion equation is written as

$$\frac{{\rm d}\gamma}{{\rm d}z}={\rm Re}\left[2{\rm i}a(z)e_2(z){\rm e}^{{\rm i}\psi}-\frac{8Ii}{I_{\rm A}(r_{\rm bo}^2-r_{\rm bi}^2)}\frac{cR'}{\omega}\times{\rm e}^{{\rm i}\psi}\langle{\rm e}^{-{\rm i}\psi}\rangle\right], \tag{14}$$

where γ is the relativistic factor and R' is the space-charge reduction factor.

For the second model, because a sever is considered as a drift area, the electromagnetic fields are entirely eliminated. Therefore, in a sever region, the beam–wave interaction equations include only the phase evolving equation and motion equation, whereas in a non-sever region, the self-consistent equations have the same forms as those for the first model.

2.4. Initial conditions

The phase of the input signal is assumed to be zero, in the meantime, the power of the input signal $P_{\rm in}$ is given, and then the initial condition of the normalized field amplitude can be expressed as

$$a(0)=\sqrt{P_{\rm in}/P_{\rm flux,2}}, \tag{15}$$

where $P_{\rm flux,2}=\dfrac{c}{2\pi}\left(\dfrac{mc^2}{q}\right)^2=1.3862\times10^9$W is a constant.

The initial condition on the phase is determined by the distribution of particle entrance times. In general, it is assumed that the entrance times are uniformly distributed over this time interval $T=2\pi/\omega$, consequently the initial condition on the phase can be written as

$$\psi_0=-\omega t_0. \tag{16}$$

The initial axial speed of a particle is assumed to be v_{z0}, and then the initial relativistic factor γ_0 is determined by the following formula:

$$\gamma_0=1/\sqrt{1-v_{z0}^2/c^2}. \tag{17}$$

Due to the space-charge effect in a helix TWT, the potential sinking effect should be considered. According to Poisson's equation, the potential at r in the beam is expressed as

$$u(r)=u_{\rm h}-\frac{Q}{2\pi\varepsilon_0}\ln\frac{R_{\rm g}}{r_{\rm o}}+\frac{\rho_0}{4\varepsilon_0}\times\left[(r_{\rm bo}^2-r^2)-r_{\rm bi}^2\ln\left(\frac{r_{\rm bo}}{r}\right)^2\right], \tag{18}$$

where $u_{\rm h}$ is the voltage on the helix, and $Q=2\pi\int_{r_{\rm bi}}^{r_{\rm bo}}|\rho(r)r{\rm d}r|$ with $\rho(r)$ being the space-charge density at radius r in the beam. Thus, v_{z0} is easily obtained.

3. Numerical results and discussion

According to the above beam–wave interaction equations and corresponding initial conditions, we have written a computational program named HTWT1D by using a fourth order Runge–Kutta algorithm. We use this program, according to the previous work,[17] to calculate wave number $k_z(z)$, interaction impedance $K(r)$ and circuit loss $\alpha_0(z)$.

As an example, we consider a helix TWT with two attenuators and a sever, part of their parameters are shown in Table 1 and Fig.1.[22] The parameters of its cold circuits can be described as follows: the mean helix radius and wall radius are 0.12446cm and 0.2794cm, respectively, and the helix pitch is 0.080137cm. The effective relative permittivity of the rods is 1.75. The tape width and thickness are 0.03556cm and 0.01524cm, respectively. The length of the interaction circuit is about 9.6cm.

In this section, the results of the HTWT1D code, according to the rigorous field theory, are presented under the condition of single-tone excitation.

Table 1. Part of parameters used in an example.

parameter	nominal value
beam radius	0.05cm
beam voltage	3000V
beam current	170mA
numbers of the attenuator and the sever	2 and 1

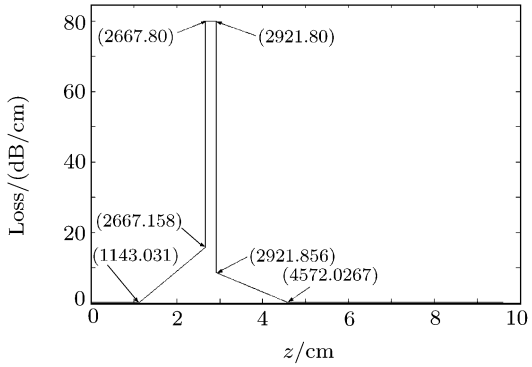


Fig.1. Attenuation profile in the Northrop Grumman TWT.

First, we observe effects of the harmonics under the condition of the different attenuator models on output power for the fundamental wave at f=5 GHz. The results are shown in Fig.2(a) and 2(b). As can be seen in the figures, the harmonics have almost no influence in the small signal area. However, they have certain effects in the nonlinear area in the case of different attenuator models. Obviously, the output power without the harmonics becomes bigger than that with the harmonics.

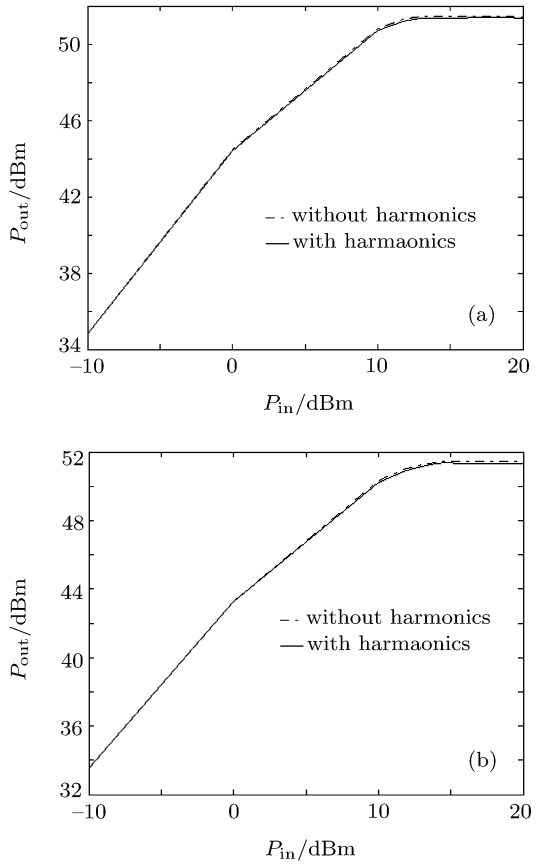


Fig.2. Comparative drive curves with or without the second harmonic for SATT model (a) and HATT model (b).

Next, with the second harmonic taken into consideration, the drive curves for different models have been compared with each other. The numerical results are shown in Fig.3. From the figure, we can conclude that in the small-signal and intermediate regimes, the values of power output at an identical input signal may be different; furthermore the HATT model predicts smaller value than the SATT model. However, the values of output power for different models have almost the same values near the saturated area.

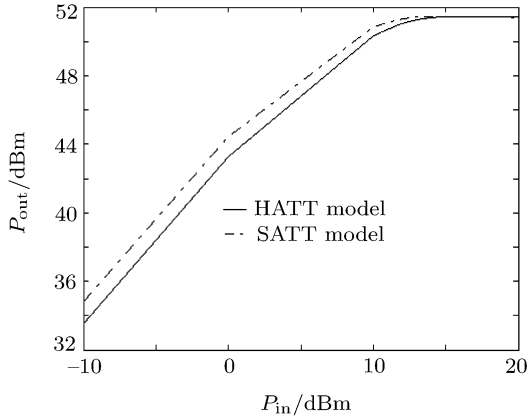


Fig.3. Comparison between the drive curves obtained from two different attenuator models in the presence of the second harmonic.

At last, in order to better study the capabilities of the HTWT1D code based on the HATT model, a small signal gain is made over a 4GHz wide band, ranging from 3 to 7 GHz. As a result, the growth rate as a function of frequency is shown in Fig.4. According to this figure, it is shown that the small signal gain at 5GHz is much higher than those at other frequencies.

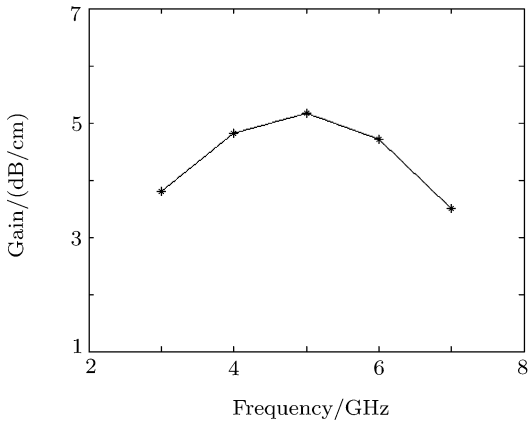


Fig.4. The small signal gain as a function of frequency.

4. Experimental verification

In order to further verify our results, we did the experiments by using a homemade helix TWT, part of

its parameters were the beam current of 114mA, beam voltage of 4200V, and beam radius of 0.32mm. Drive curves are plotted in Fig.5. From the figure, it is clear that the SATT model and the HATT model each can yield a similar variation with input power at 12GHz, whereas the results predicted from the HATT model are much closer to the experimental data than those obtained from the SATT model. Hence, the HATT model is adopted in the simulation of saturated gain characteristics, and then comparison of saturated gain between the results from the HTWT1D and the experimental data is shown in Fig.6. The calculated results are in good agreement with experimental data.

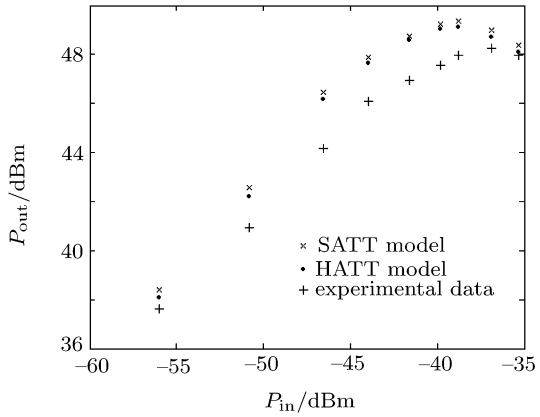


Fig.5. Comparisons of drive curves from SATT and HATT models separately with experimental data.

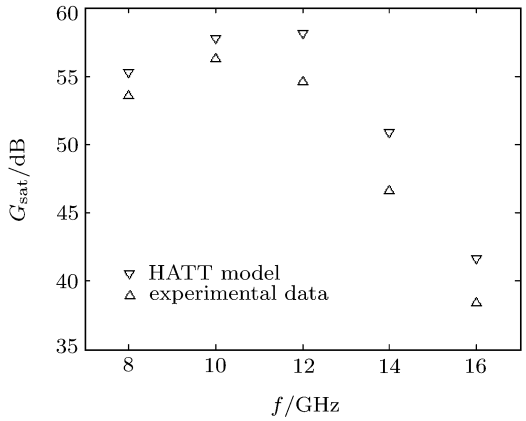


Fig.6. Comparison of the saturated gain determined by HTWT1D with experimental data.

5. Conclusion

In this paper we have described a one-dimensional nonlinear beam–wave interaction based on a rigorous field theory, and for the purpose of practical simulation, the concrete expression of the complex function is derived and potential sinking effect is also considered. Thus, two different physical models of attenuator and sever have been set up and incorporated into the simulation code HTWT1D. The simulation results are compared with the measured results, and they accord with each other in overall tendency.

However, in the course of the work, the discrepancies between HTWT1D and experimental data are exposed. The discrepancies, to our knowledge, originate mainly from the two aspects. One is one-dimensional approximation. In order to prove our theory, a guiding magnetic field that is approximately 1.5 times the Brillouin field in strength should be used, because the electron motion is largely confined to one dimension. Unfortunately, in fact, the devices used in our simulations were a solenoid focused with an axial magnetic field only close to the Brillouin field in strength. Hence the electron motion cannot be described approximately by one dimension. And the other is attenuation profiles at different frequencies. As is known, attenuation increases with operational frequency. However, we cannot obtain accurate data from the designers at different frequencies.

To summarize, our results are in good agreement with the measured data on the whole. Thereby these calculated results provide a strong basis for designing broadband and high gain helix TWTs.

References

[1] Gong Y B, Zhang Z, Wei Y Y, Meng F B, Fan Z K and Wang W X 2004 *Acta Phys. Sin.* **53** 3990 (in Chinese)

[2] Liu G Z, Huang W H, Shao H and Xiao R Z 2006 *Chin. Phys.* **15** 600

[3] Zhao D, Ding Y G, Sun P and Wang J H 2006 *Acta Phys.*

Sin. **55** 2389 (in Chinese)
[4] Pierce J R 1950 *Traveling Wave Tubes* (Princeton, NJ: Van Nostrand) p109
[5] Nordsieck A 1953 *Proc. IRE* **41** 630
[6] Tien P K, Walker L R and Wolontis V M 1955 *Proc. IRE* **43** 260
[7] Rowe J E 1956 *IRE Transactions—Electron Devices* **3** 39
[8] Rowe J E 1965 *Nonlinear Electron–Wave Interaction Phenomenon* (New York: Academic) p19
[9] Liu S G, Li H F, Wang W X and Mo Y L 1985 *Introduction to Microwave Electronics* (Beijing: National Defence Industry Press) p334 (in Chinese)
[10] Freund H P and Zaidman E G 1997 *Plasma Science* 1997 *IEEE Conference Record—Abstracts* 1997 p197
[11] Antonsen Jr T M and Levush B 1997 *NRL Memo Report* NRL/FR/6840-97-9845 (Washington, DC: NRL)
[12] Antonsen Jr T M and Levush B 1998 *IEEE Trans. Plasma Science* **26** 774
[13] Wöhlbier J G, Booske J H and Dobson I 2002 *IEEE Trans. Plasma Science* **30** 1063
[14] Li B and Yang Z H 2003 *Chin. Phys.* **12** 1235
[15] Li J Q and Mo Y L 2006 *Acta Phys. Sin.* **55** 4117 (in Chinese)
[16] Xie H Q and Liu P K 2007 *Chin. Phys.* **16** 766
[17] Duan Z Y, Gong Y B, Wei Y Y, Wang W X and Huang M Z 2004 *Int. J. Electronics* **91** 309
[18] Yan T C 1986 *Acta Electronica Sin.* **14** 67 (in Chinese)
[19] Swift-Hook D T 1958 *Proc. IRE* **105b** 747
[20] Duan Z Y, Gong Y B, Wang W X, Wei Y Y and Huang M Z 2004 *IEEE Trans. Plasma Science* **32** 2184
[21] Xie C F and Rao K J 1987 *Electromagnetic Field and Waves* (Edition 2) (Beijing: Publishing House of Higher Education) p324 (in Chinese)
[22] Freund H P 2000 *IEEE Trans. Plasma Science* **28** 748